Journal of Power Sources 185 (2008) 1122–1130

Contents lists available at ScienceDirect

Journal of Power Sources

journal homepage: www.elsevier.com/locate/jpowsour

Anode gas recirculation behavior of a fuel ejector in hybrid solid oxide fuel cell systems: Performance evaluation in three operational modes

Yinhai Zhu [a,b], Wenjian Cai [b,*], Yanzhong Li [a], Changyun Wen [b]

[a] School of Energy and Power Engineering, Xi'an Jiaotong University, Xi'an 710049, PR China
[b] School of Electrical and Electronic Engineering, Nanyang Technological University, 639798 Singapore, Singapore

ARTICLE INFO

Article history:
Received 10 June 2008
Received in revised form 15 July 2008
Accepted 16 July 2008
Available online 23 July 2008

Keywords:
SOFC
Anode gas recirculation
Ejector
Modeling
Performance monitoring
Fault detection

ABSTRACT

In this paper, a theoretical model for the performance monitoring and fault detection of fuel ejectors in the hybrid solid oxide fuel cell (SOFC) system is proposed. The procedures of using the model to analyze ejector properties such as the primary mass flow rate, the secondary mass flow rate, the recirculation ratio and steam to carbon ratio (STCR) are introduced. Based on the model, the anode gas recirculation performances of a hybrid SOFC system are studied under various operating conditions. Results show that the model can be used to evaluate the performance of ejector not only in the critical mode but also in the subcritical and back flow modes, which is especially useful at SOFC off-design operating conditions such as start up, load changes and shut down.

1. Introduction

Fuel cells, which convert chemical energies, such as hydrogen, methanol, ethanol, formic acid, and methane, into electric energy, possess several potential advantages over conventional combustion power generation processes including higher efficiency, lower emissions, and higher power density. Fuel cell technique has been considered to be one of the best candidates for the future power generation and has drawn intensive research interests in recent years [1,2]. Among several fuel cell schemes, solid oxide fuel cell (SOFC) is a potential alternative in the distributed power generation for domestic, commercial and industrial sectors. In the anode side of an SOFC stack, the exhaust is rich in steam (about 40–45% in mass) and high in temperature (around 900 °C), which can be recycled by means of an ejector to provide enough steam to prevent carbon deposition and sufficient heat for endothermic reforming reactions in the cell and reformer [3,4]. Another ejector can also be applied in the cathode side to recover part of the exhausted gases to replace a high temperature recuperator [5,6]. In these ejectors, a high pressure gas called as the primary flow is used to entrain the anode or cathode exhausts. Since the ejector is an important component in the recirculation cycle of an SOFC system, a clear understanding of its working principle and performance characteristic is required.

Ejectors have been under investigation for many years, and several modeling techniques are available, especially in the areas of refrigeration and chemical engineering [7–9]. Due to the features of high recirculation ratio, low pressure increment and over heated working gases, however, very few existing modeling techniques can be directly applied to SOFC systems.

Marsano et al. [10] developed an SOFC ejector model by using 1D modeling technique. The developed model can be used to deal with both on-design and off-design performance evaluations. However, this model does not account for the operation conditions when the amount of entrained anode recycle gas is very small at very low primary flow pressure. Later on, Ferrari et al. [11] improved the modeling technique by dividing the ejector into serials of calculation cells where the governing equations were numerically solved by 1D-CFD method as well as "lumped volume" treatment. This improvement makes the model capable of predicting the transient behavior. Recently, Zhu et al. [12] proposed a new modeling technique for fuel ejectors by employing a 2D function to compute fluid velocity near the ejector inner walls. The developed model can be applied in both geometry design and performance simulation of fuel ejectors. However, the model cannot accurate predict the ejector performance when it works at low primary flow pressure.

According to the primary flow pressure, the ejector performance can be divided into three operational modes, i.e., back flow,

* Corresponding author. Tel.: +65 6790 6862; fax: +65 6793 3318.
E-mail address: ewjcai@ntu.edu.sg (W. Cai).

0378-7753/$ – see front matter © 2008 Elsevier B.V. All rights reserved.
doi:10.1016/j.jpowsour.2008.07.027

Nomenclature

A	area (m^2)
C_p	specific heat of gas at constant pressure ($J\,kg^{-1}\,K^{-1}$)
D	diameter (m)
FC	fuel cell
k	specific heat ratio of gas
m	mass flow rate ($kg\,s^{-1}$)
M	Mach number
M_{ml}	Mach number of the mixing layer at Section 3
Mo	molecular weight ($kg\,mol^{-1}$)
n	molar flow rate ($mol\,s^{-1}$)
n_v	exponent of the 2D curve
P	pressure (Pa)
r, R	radius (m)
R_g	gas constant ($J\,kg^{-1}\,K^{-1}$)
R_u	universal gas constant ($J\,mol^{-1}\,K^{-1}$)
T	temperature (K)
v, V	velocity ($m\,s^{-1}$)

Greek letters

ζ_{exp}	coefficient accounting for friction loss during the mixing process
ρ	density ($kg\,m^{-3}$)
Ψ_P	isentropic coefficient of primary flow
ω	recirculation ratio (m_S/m_P)

Subscripts

P	primary flow (i.e. inlet fuel)
S	secondary flow (i.e. anode recycling gas)
t	nozzle throat
0	ejector inlet
1	primary flow at nozzle throat
2	nozzle exit
3	mixing chamber inlet
4	mixing chamber outlet
5	ejector exit

Superscripts

i	chemical component

subcritical and critical modes [8,13]. The ejector may work in the subcritical mode or even back flow mode during start up, load changes and shut down. In these cases, the ejector performance characteristic is more complex than that in the critical mode. Noting that both the heat required for the reforming reactions and steam for avoiding carbon deposition are supplied by the entrained anode gas, unexpected fluctuations in fuel cell system could occur and then the system might run under some "dangerous" conditions. Therefore, it is essential to develop a simple and accurate fuel ejector model for the performance monitoring and fault detection of fuel ejectors in all the three operational modes.

In this paper, we aim to develop a theoretical model for fuel ejectors in the hybrid SOFC system for performance monitoring and fault detection in all the three operational modes. Governing equations for computing the mass flow rate, recirculation ratio and STCR are first derived based on the thermodynamic and fluid dynamic principles. A method to determine the two key parameters P_{PE} and P_{PC} is proposed. The model applications in the performance monitoring and fault detection for fuel ejectors are discussed. A hybrid SOFC system integrated with a fuel ejector at the anode side is also studied using the proposed model. The anode gas recirculation behaviors in all the three operational modes are obtained and analyzed. Results show that the model can be used to evaluate the performance of ejectors not only in the critical mode but also in the subcritical and back flow modes. This property is especially useful to analyze the performance of an off-design operating SOFC system.

2. Fuel ejector in anode gas recirculation SOFC system

2.1. SOFC system description

A typical anode gas recirculation SOFC system, which mainly consists of three components: an ejector, a reformer and a fuel cell stack, is schematically shown in Fig. 1. High pressure fuel (primary flow) passes through the ejector to entrain the low pressure anode exhaust (secondary flow). The primary flow and the secondary flow mix in the mixing chamber. The mixed stream shocks in the diffuser and then enters into the connected reformer. Inside the reformer, highly endothermic reactions take place:

$$\text{Reforming}: \ CH_4 + H_2O \leftrightarrow CO + 3H_2 \tag{1a}$$

$$\text{Shifting}: \ CO + H_2O \leftrightarrow CO_2 + H_2 \tag{1b}$$

The reformed fuel is fed to the anode side of FC stack, while air is supplied to the cathode side. In the cathode, oxygen ions passing through the electrolyte layer react with hydrogen, and the electrons are released. These electrons pass through the external circuit and reach the cathode electrolyte layer to make the circuit close. The reactions inside the FC stack can be summarized as follows:

$$\text{Reforming}: \ CH_4 + H_2O \leftrightarrow CO + 3H_2 \tag{2a}$$

$$\text{Shifting}: \ CO + H_2O \leftrightarrow CO_2 + H_2 \tag{2b}$$

$$\text{Electrochemical}: \ H_2 + \tfrac{1}{2}O_2 \rightarrow H_2O \tag{2c}$$

In the anode gas recirculation SOFC system, STCR, which is a very important parameter to evaluate carbon deposition in the reformer and FC stack, is defined as follows [10]

$$\text{STCR} = \frac{n_{H_2O}}{n_{CO} + n_{CH_4}} \tag{3}$$

In terms of fuel ejectors in the anode gas recirculation cycle, the STCR can be computed by:

$$\text{STCR} = \frac{n_{S,0}^{H_2O} / \sum_i n_{S,0}^i \text{Mo}^i}{\left(n_{S,0}^{CO} / \sum_i n_{S,0}^i \text{Mo}^i \right) + \left(n_{P,0}^{CH_4} / \sum_i n_{P,0}^i \text{Mo}^i \omega \right)} \tag{4}$$

where the recirculation ratio, ω, is defined as

$$\omega = \frac{m_S}{m_P} \tag{5}$$

where m_S, m_P are the mass flow rates of the primary flow and the secondary flow, respectively.

2.2. Ejector operational modes

The ejector's recirculation ratio is strongly influenced by three pressures: primary flow pressure, secondary flow pressure and back pressure (pressure of gas in the reformer). Since the system load of an SOFC is usually adjusted through the primary flow pressure, its effect on the recirculation ratio is shown in Fig. 2 [13,14]. Accordingly, the ejector performance can be divided into three operational modes: back flow, subcritical and critical. The primary mass flow rate increases with the primary flow pressure in all the three modes. In contrast, the behavior of secondary flow is different in each mode:

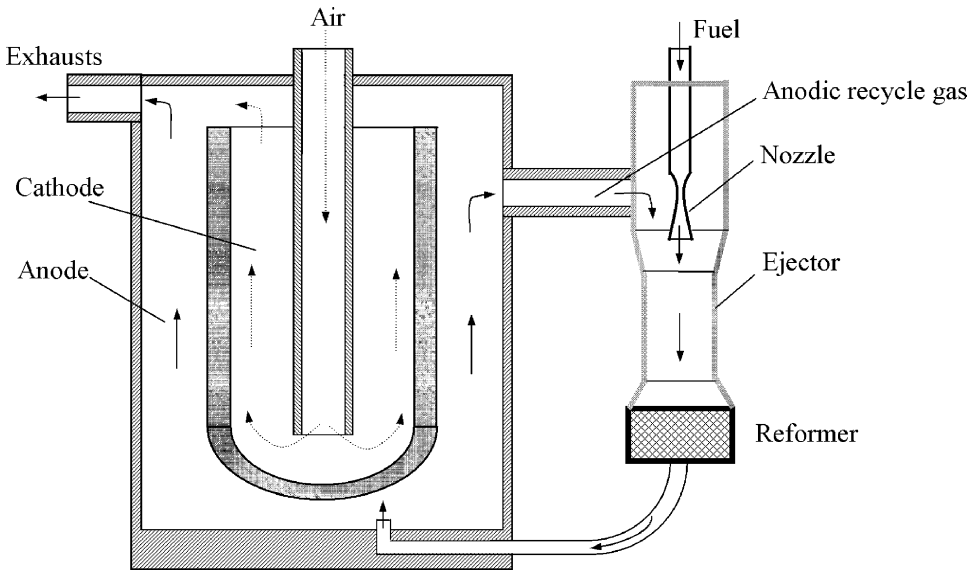

Fig. 1. Simplified sketch of an SOFC module.

Back flow mode: At low primary flow pressure, no secondary flow is entrained into the ejector.
Subcritical mode: The ejector starts entraining the secondary flow as the primary flow pressure rises to P_{PE}. The recirculation ratio is very sensitive to the primary flow pressure in the subcritical mode.
Critical mode: The secondary flow shocks in the ejector and reaches the critical mode when the primary flow pressure is equal to P_{PC}. In the critical mode, the secondary flow rate decreases first and then is near constant in the high pressure region.

Detailed flow field and pressure distribution of an ejector in the three operational modes are shown in Fig. 3(a)–(c), respectively. In Fig. 3(a), the ejector works at the back flow mode as the primary flow pressure ranges from 0 to P_{PE}. The pressure in the mixing chamber is higher than that of the secondary flow, resulting in part of the primary flow is reversed and no shock occurs in the ejector.

In the subcritical mode ($P_{PC} > P_{P,0} > P_{PE}$), the secondary flow is entrained into the ejector due to the pressure in the mixing chamber is lower than that of the secondary flow. There is only one shock in the diffuser (single-choking [8]).

In the critical mode ($P_{P,0} \geq P_{PC}$) as described in Fig. 3(c), the primary flow expands after the nozzle exit introducing a series of oblique shocks in the suction chamber, and accelerates the secondary flow to choking condition at the mixing chamber, then the mixed flow shocks again in the diffuser. This phenomenon is known as double-choking [8]. Since the secondary flow shocks at the mixing chamber inlet, the ejector working at the critical mode is more stable than the other two modes.

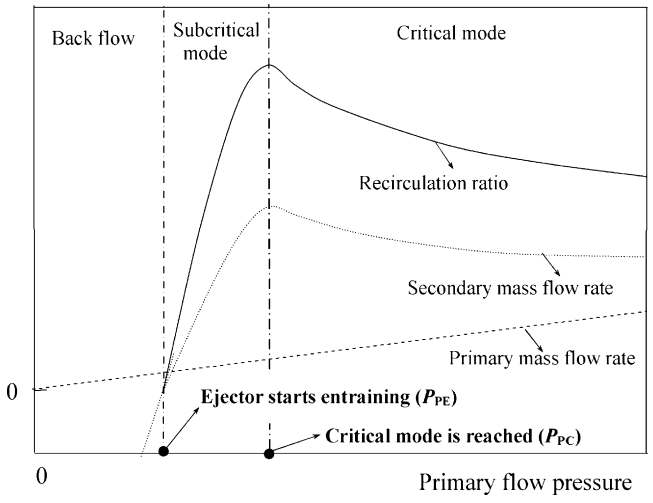

Fig. 2. Ejector performance at different primary flow pressures.

3. Theoretical model development

In this study, it is assumed that the ejector meets the following conditions:

1. Both the primary and the secondary flows are ideal gas inside adiabatic ejector walls.
2. The isentropic relations are used for simplicity in deriving the model.
3. The primary flow velocity is uniform in the radial direction, while velocity of the secondary flow is non-uniformly distributed inside the ejector.
4. The primary flow is fully heated to the temperature of the secondary flow and the lost heat energy of secondary flow is negligible (i.e. $T_{S,3} = T_{S,0}$; $T_{P,3} = T_{S,0}$) [12].
5. Pressure and temperature of both the primary and the secondary flows are uniformly distributed in the radial direction of the ejector.
6. The frictional loss during the mixing process is taken into account by a coefficient.

3.1. Relations between ejector inlet and Section 3

Using the isentropic flow laws and the energy balance equation, the mass flow rate of the primary flow through the nozzle is [12]

$$m_P = A_t \overline{\rho_{P,0}} (\psi_P k_P R_{g,P} T_{P,0})^{0.5} \left(\frac{2}{k_P + 1}\right)^{(k_P+1)/(2(k_P-1))} \quad (6a)$$

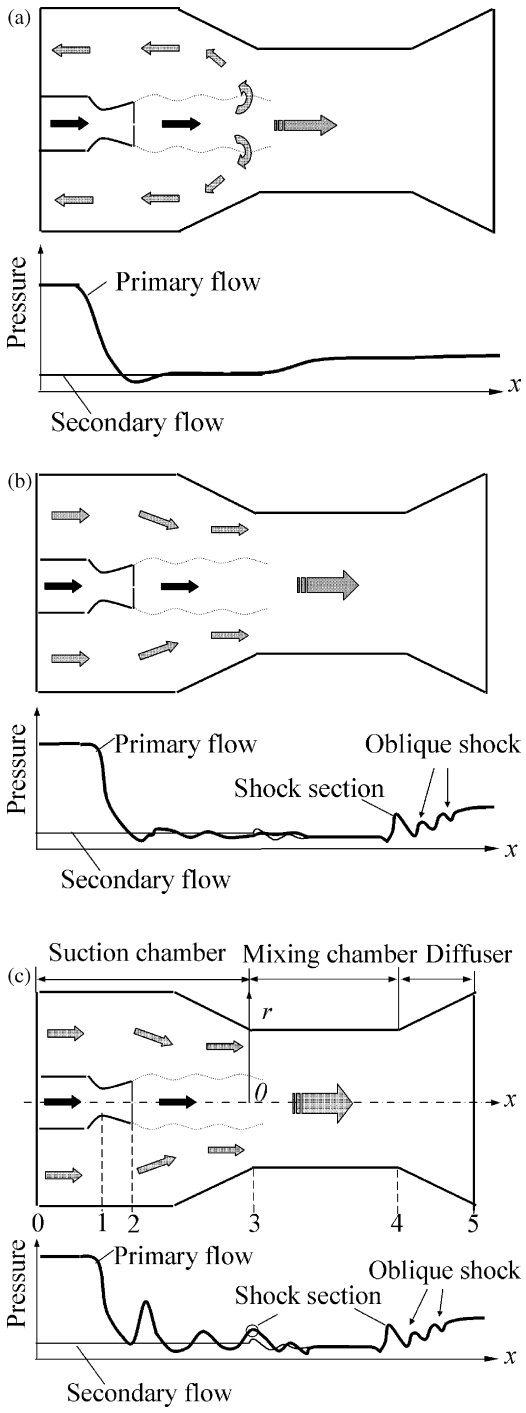

Fig. 3. Schematic diagram showing pressure distribution along ejector in different modes. (a) Back flow, (b) subcritical mode and (c) critical mode.

where ψ_P is the coefficient relating to the isentropic efficiency of the primary flow; $T_{P,0}$ is the fuel inlet temperature; the average gas constant and density of the inlet fuel are defined as

$$R_{g,P} = \frac{R_u \sum_i n^i_{S,0}}{\sum_i n^i_{S,0} Mo^i} \tag{6b}$$

and

$$\overline{\rho_{P,0}} = \frac{P_{P,0}}{R_{g,P} T_{P,0}} = \frac{P_{P,0}}{T_{P,0}} \frac{\sum_i n^i_{P,0} Mo^i}{R_u \sum_i n^i_{P,0}} \tag{6c}$$

for a mixture inlet fuel, respectively.

Relations between the Mach number, velocity, flow diameter of the primary flow at Section 3 and the inlet boundary conditions $P_{P,0}$, $P_{S,0}$, $T_{S,0}$ can be written as

$$M_{P,3} = \left(\frac{2}{k_P - 1}\right)^{0.5} \left[\left(\frac{P_{P,0}}{P_{S,0}}\right)^{(k_P-1)/k_P} - 1\right]^{0.5} \tag{7}$$

$$V_{P,3} = \left(\frac{2k_P R_{g,P} T_{S,0}}{k_P - 1}\right)^{0.5} \left[\left(\frac{P_{P,0}}{P_{S,0}}\right)^{(k_P-1)/k_P} - 1\right]^{0.5} \tag{8}$$

$$D_{P,3} = \frac{D_t {M_{P,3}}^{-0.5}}{\zeta_{exp}} \left(\frac{2 + (k_P - 1){M_{P,3}}^2}{2 + (k_P - 1)}\right)^{(k_P+1)/4(k_P-1)} \tag{9}$$

where $M_{P,3}$, and $V_{P,3}$ are the Mach number and velocity of the primary flow at Section 3, respectively; $D_{P,3}$ is the diameter of the flow area of the primary flow at Section 3. The details of deriving Eqs. (7) and (9) are presented in Appendix B of Ref. [12].

In Section 3, the primary flow and the secondary flow are separated by a mixing layer [12]. Inside the layer is the primary flow which is assumed to have a constant velocity in the radial direction, and the secondary flow is outside the layer with nonlinear velocity distribution. A 2D velocity function for the primary flow and secondary flow in Section 3 is defined as follows [12]:

$$v_r = \begin{cases} V_{P,3} & (0 \le r \le R_{P,3}) \\ V_{P,3}(1 - r/R_3)^{1/n_v} & (R_{P,3} < r \le R_3) \end{cases} \tag{10}$$

where $R_{P,3}$ means the radius of the mixing layer in Section 3; R_3 is the radius of the mixing chamber; n_v is the exponent of the velocity function. Considering the velocity and the radius of the mixing layer are $v_r = M_{ml}\sqrt{kR_g T_{S,0}}$ and $r = R_{P,3} = D_{P,3}/2$, respectively [12], and substituting these values and $V_{P,3} = M_{P,3}\sqrt{kR_g T_{S,0}}$ into Eq. (10), we obtain

$$n_v = \frac{\ln(1 - R_{P,3}/R_3)}{\ln(M_{ml}/M_{P,3})} \tag{11}$$

By expressing the mean mass flow rate of the secondary flow at Section 3 as

$$m_S = \int_{R_{P,3}}^{R_3} \bar{\rho} v_r \, dA \tag{12}$$

it then can be obtained through evaluating the integral of Eq. (12),

$$m_S = 2\pi V_{P,3} \overline{\rho_{S,0}} \left[\frac{n_v {R_3}^2}{n_v + 1}\left(1 - \frac{R_{P,3}}{R_3}\right)^{(n_v+1)/n_v} - \frac{n_v R_3^2}{2n_v + 1}\left(1 - \frac{R_{P,3}}{R_3}\right)^{(2n_v+1)/n_v}\right] \tag{13a}$$

where the average density of the secondary flow is given by

$$\overline{\rho_{S,0}} = \frac{P_{S,0}}{R_{g,S} T_{S,0}} = \frac{P_{S,0}}{T_{S,0}} \frac{\sum_i n^i_{S,0} Mo^i}{R_u \sum_i n^i_{S,0}} \tag{13b}$$

3.2. Mixing process between Sections 3 and 4

The primary flow mixes with the secondary flow in the mixing chamber. The mass, energy and momentum conservation equations for the mixing process are introduced as follows:

Mass conservation equation:

$$\frac{P_4 V_4 A_3}{R_{g,m} T_4} = m_P + m_S \tag{14}$$

where P_4, T_4 and V_4 are the pressure, temperature and velocity of the mixed flow at Section 4, respectively; the average gas constant of the mixed flow is

$$R_{g,m} = \frac{R_u \sum_i n_m^i}{\sum_i n_m^i \mathrm{Mo}^i} \tag{15}$$

Energy conservation equation:

$$(m_P + m_S)(C_p T_4 + \tfrac{1}{2} V_4^2) = m_P C_p T_{P,0} + m_S C_p T_{S,0} \tag{16}$$

Momentum conservation equation:

$$P_4 A_3 + \frac{V_4}{\varphi_m}(m_P + m_S) = (m_P V_{P,3} + P_{P,3} A_{P,3}) + (m_S V_{S,3} + P_{S,3} A_{S,3}) \tag{17}$$

where φ_m expresses a coefficient taking account the frictional loss in the mixing process; $A_{S,3}$ is the flow area of the secondary flow at Section 3 ($A_{S,3} = A_3 - A_{P,3}$); $V_{S,3}$ and $P_{S,3}$ which are the velocity and pressure of the secondary flow in Section 3, can be determined by Eqs. (18) and (19), respectively:

Considering $V_{S,3} = m_S/(\overline{\rho_{S,0}} A_{S,3})$, and invoking Eq. (13a), we have

$$V_{S,3} = \frac{2\pi V_{P,3}}{A_{S,3}} \left[\frac{n_v R_3^2}{n_v + 1} \left(1 - \frac{R_{P,3}}{R_3}\right)^{(n_v+1)/n_v} - \frac{n_v R_3^2}{2n_v + 1} \left(1 - \frac{R_{P,3}}{R_3}\right)^{(2n_v+1)/n_v} \right] \tag{18}$$

using the isentropic flow and energy conservation law for the secondary flow from Sections 0 to 3, we have

$$\frac{P_{S,0}}{P_{S,3}} = \left(1 + \frac{k_S - 1}{2} M_{S,3}^2\right)^{k_S/(k_S-1)} \tag{19}$$

where $M_{S,3} = V_{S,3}/\sqrt{k R_{g,S} T_{S,0}}$.

3.3. Pressure diffusing from Section 4 to Section 5

In the subcritical and critical modes, the mixed flow will shock at the end of the mixing chamber and in the diffuser. After this shock, the kinetic energy of the mixed flow is converted into pressure. Assuming the pressure diffusing is an isentropic process, the pressure at the exit of the diffuser P_5 can be expressed by

$$\frac{P_5}{P_4} = \left(1 + \frac{k_m - 1}{2} M_4^2\right)^{k_m/(k_m-1)} \tag{20}$$

The Mach number of the mixed flow at Section 4 is calculated using the following relation:

$$M_4 = \frac{V_4}{\sqrt{k_m R_{g,m} T_4}} \tag{21}$$

where the specific heat ratio of the fuel in the mixing chamber is defined as

$$k_m = \frac{C_p}{C_p - R_{g,m}} \tag{22}$$

Note that some geometry properties of the ejector such as the converging and diverging angles and the chamber lengths are not accounted in the model due to the employment of 1D modeling technique. Therefore, the influence of these properties on the ejector performance is not revealed in this model. Fortunately, this limitation is not critical since these geometry properties will not seriously affect on the ejector performance.

4. Operational mode estimation

The mass flow rate of the primary flow and secondary flow can be analyzed by the set of equations from Eqs. (6) to (22). Substituting these values into Eqs. (4) and (5), a theoretical fuel ejector model for the anode gas recirculation performance evaluation is finally constructed. As stated in Fig. 2, the ejector performance is divided into the three operational modes by the two values of P_{PE} and P_{PC}; and the anode gas recirculation behavior is quite different among the three operational modes. In order to better monitor the fuel ejector performance, it is necessary to estimate first which mode the fuel ejector is in, and then to evaluate the performance parameters such as the recirculation ratio and STCR.

4.1. Determine P_{PE}

The primary flow starts to entrain the secondary flow when the primary flow pressure reaches P_{PE}. In this condition, the mass flow rate of the secondary flow is zero, i.e. $m_S = 0$; $V_{S,3} = 0$; $M_{S,3} = 0$. Substitute these values into Eqs. (14) and (16)–(19), the governing equations for the flow in the mixing chamber are updated as follows:

$$\frac{P_4 V_4 A_3}{R_{g,m} T_4} = m_P \tag{23}$$

$$m_P(C_p T_4 + \tfrac{1}{2} V_4^2) = m_P C_p T_{P,0} \tag{24}$$

$$P_4 A_3 + \frac{V_4 m_P}{\varphi_m} = (m_P V_{P,3} + P_{S,0} A_{P,3}) + (P_{S,0} A_{S,3}) \tag{25}$$

$$P_{S,3} = P_{S,0} \tag{26}$$

$$V_{S,3} = 0 \tag{27}$$

Due to the non-linearity and close coupling of these equations, an iterative procedure is required for determining P_{PE} as shown in Fig. 4(a).

4.2. Determine P_{PC}

The fuel ejector works in the critical mode as the primary flow pressure is greater than P_{PC}. In this operating condition, the secondary flow is accelerated by the primary flow and always shocks at the mixing chamber inlet. At the critical mode, it can be reasonably assumed that only the layer between the primary flow and secondary flow in Section 3 is in the choking condition, i.e. $M_{ml} = 1$ [12]. Substituting this into Eq. (11), we have

$$n_v = \frac{\ln(1 - R_{P,3}/R_3)}{\ln(1/M_{P,3})} \tag{28}$$

Using this condition, a detailed calculation flowchart for determining P_{PC} is given in Fig. 4(b).

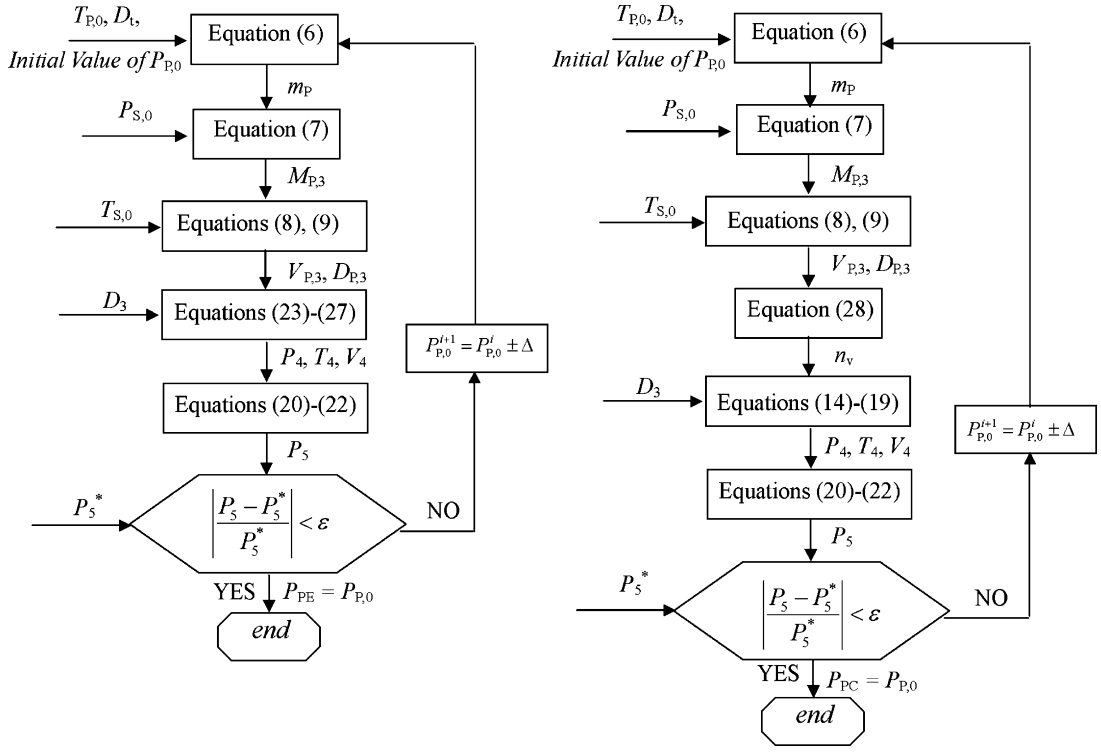

Fig. 4. Flowchart for determining two key primary flow pressures. (a) For determining P_{PE} and (b) for determining P_{PC}.

5. Application procedures

For a given ejector geometry, the anode gas recirculation performance depends on $P_{P,0}$ and $P_{S,0}$, $T_{P,0}$ and $T_{S,0}$, and the chemical composition of inlet fuel and anode recycle gas. The model application procedure in performance monitoring and fault detection is introduced as follows:

(1). *Estimate which operational mode the ejector is in*: the ejector performance is divided into the three operational modes by P_{PE} and P_{PC}, which can be determined by the flowchart shown in Fig. 4. Operational mode of the fuel ejector is

$$\text{Operational mode} = \begin{cases} \text{back flow mode;} & (0 < P_{P,0} < P_{PE}) \\ \text{subcritical mode;} & (P_{PE} \le P_{P,0} < P_{PC}) \\ \text{critical mode;} & (P_{P,0} \ge P_{PC}) \end{cases} \quad (29)$$

(2). *Compute m_P and m_S*: the mass flow rate of the primary flow m_P can be computed from Eq. (6a) as the fuel ejector works in all the three modes. But for computing the mass flow rate of the secondary flow m_S, the governing equation is different in the three modes. In addition, as shown in Fig. 2, it is found that m_S is approximately linear with the primary flow pressure in the subcritical mode and satisfies the boundary conditions: $P_{P,0} = P_{PE}$, $m_S = 0$ and $P_{P,0} = P_{PC}$, $m_S = f(P_{PC})$. In order to reduce the calculation time, a linear function is defined to approach the secondary mass flow rate in the subcritical mode by considering the boundary conditions. Governing equations for the secondary mass flow rate in the three operational modes are expressed by:

$$m_S = \begin{cases} - & (0 < P_{P,0} < P_{PE}) \\ f(P_{PC})\dfrac{P_{P,0} - P_{PE}}{P_{PC} - P_{PE}} & (P_{PE} \le P_{P,0} < P_{PC}) \\ f(P_{P,0}) & (P_{P,0} \ge P_{PC}) \end{cases} \quad (30)$$

where f is the function of m_S. Inputs of the function are the ejector geometries D_t and D_3, and the operation conditions $P_{P,0}$, $P_{S,0}$, $T_{P,0}$ and $T_{S,0}$; and output is m_S. The detailed computation procedure is given in Fig. 5.

(3). *Determine the recirculation ratio and STCR*: the recirculation ratio and STCR can be computed from Eqs. (4) to (5) once m_P and m_S are determined.

6. Results and discussions

As an example, Table 1 shows the typical values for an anode gas recirculation SOFC system analyzed in [12]. Starting with these

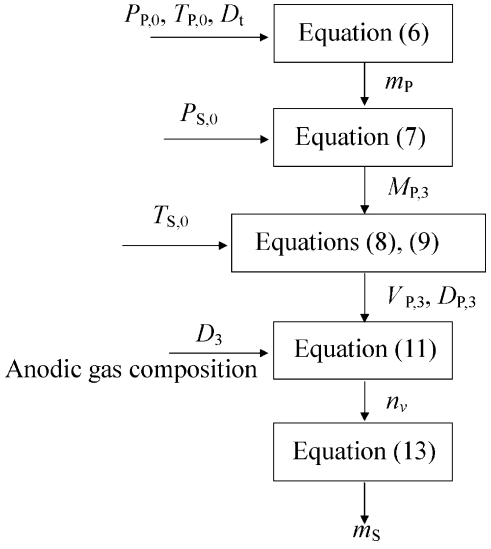

Fig. 5. Calculation flowchart for ejector performance simulation.

Table 1
On-design values of the ejector and SOFC

Parameter	Value
Fuel inlet	
Composition (molar, %)	
CH_4	100
Flow rate (kg s^{-1})	0.0094
Pressure (bar)	10.06
Temperature (K)	673
Anode gas recirculation gas	
Composition (molar, %)	
H_2	4.895
CO	3.785
H_2O	61.74
CO_2	29.58
Pressure (bar)	3.8
Temperature (K)	1280
Fuel cell parameters	
Cathode thickness (cm)	0.035
Electrolyte thickness (cm)	0.017
Anode thickness (cm)	0.030
Overall cell area (m^2)	95
Fuel cell operation conditions	
Fuel utilization	0.85
FC pressure (bar)	3.80
FC pressure loss (kPa)	5.7
Air inlet pressure (bar)	3.84
Air inlet temperature (K)	1000
Air flow rate (kg s^{-1})	0.47

data, the influences of the fuel inlet conditions, the cell operation pressure and temperature, the fuel utilization, etc., on the hybrid SOFC system are carefully studied based on the proposed fuel ejector model. During the simulation, the SOFC model developed by Costamagna et al. [15] is adopted, which allows the evaluation of both on-design and off-design behavior of the SOFC system. The main assumptions in this study are listed as follow:

1. Temperature within all the components of SOFC system is uniformly distributed.
2. Cathode flow is composed of 21% O_2 and 79% N_2. Fuel is pure CH_4.
3. The reforming and shifting reactions are at equilibrium in the reformer and FC stack.
4. Temperature of the gases at the outlet of the reformer and FC stack are equal to the reformer and FC stack temperature, respectively.
5. The pressure loss in FC stack is equal to 1.5% of the FC operation pressure.
6. The concentration loss is fixed at 1.5×10^{-7} Ω.

A design value of STCR equals to 2.4 and must be higher than 2 to avoid the carbon deposition [2,16]. The fuel utilization coefficient U_f is define as

$$U_f = \frac{n_{H_2}^{consumed}}{n_{H_2}^{in} + n_{CO}^{in} + 4n_{CH_4}^{in}} \quad (31)$$

where $n_{H_2}^{consumed}$ represents the reaction rate of H_2 in the FC stack, and $n_{H_2}^{in}$, n_{CO}^{in}, $n_{CH_4}^{in}$ are molar flow rate of H_2, CO and CH_4 into the FC stack, respectively.

6.1. P_{PE} and P_{PC}

P_{PE} and P_{PC} are affected by the operating conditions. Effects of the primary flow temperature, and the secondary flow temperature and pressure on P_{PE} and P_{PC} are presented in Fig. 6(a)–(c), respectively.

Fig. 6(a) shows the behavior of P_{PE} and P_{PC} at different primary flow temperatures. It is observed that both P_{PE} and P_{PC} increase with the primary flow temperature. This can be explained as follows:

(1) Higher temperature means lower density for a fixed pressure gas;
(2) Gas dynamic viscosity increases when temperature increases and pressure is constant.

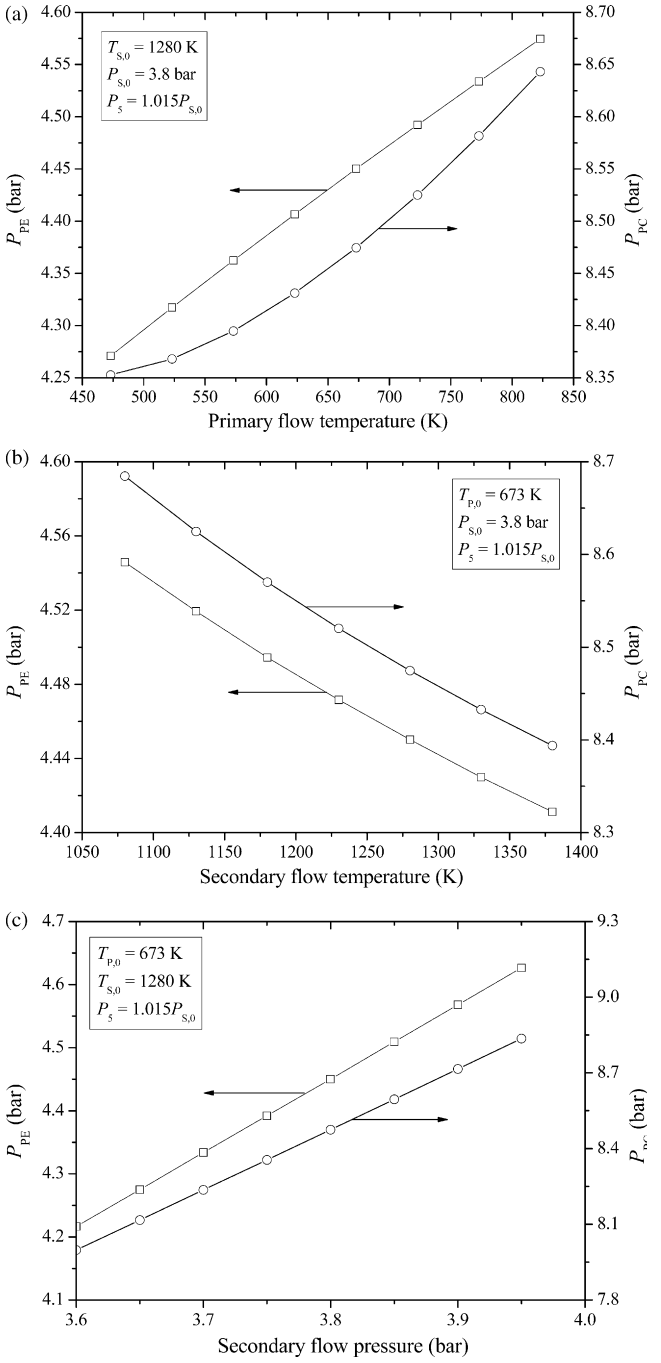

Fig. 6. Influences on P_{PE} and P_{PC} of: (a) primary flow temperature, (b) secondary flow temperature and (c) secondary flow pressure.

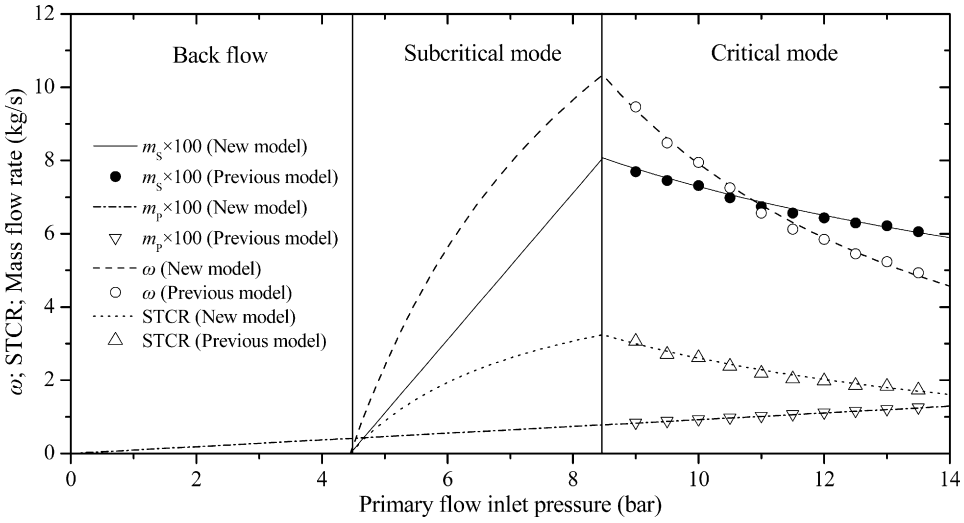

Fig. 7. Fuel ejector performance at three operational modes.

Both lead to less mass flow rate of the primary flow according to the fluid dynamics principles.

The relations between the two pressure values and the secondary flow temperature are shown in Fig. 6(b). Both P_{PE} and P_{PC} decrease with the secondary flow temperature, which implies that the ejector will start to entrain the secondary flow earlier if the secondary flow temperature is higher.

In Fig. 6(c), it is seen that P_{PE} and P_{PC} increase as the secondary flow pressure increases. Noting that value of the ejector exit pressure (P_5) remains 1.015 times of the secondary flow pressure, we conclude from Fig. 6(a) to (c) that the fuel ejector starts to entrain the secondary flow once the primary flow pressure is 1.11–1.19 times of the ejector exit pressure, and will work in the critical mode as the primary flow pressure is greater than 2.17–2.25 times of the ejector exit pressure.

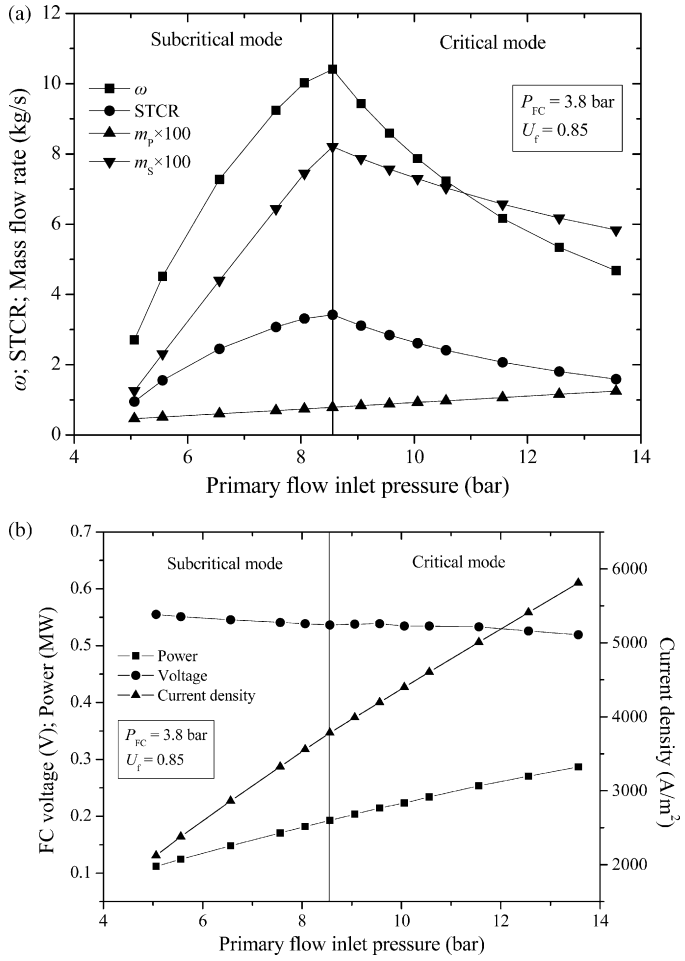

Fig. 8. Performance of a hybrid SOFC at on-design conditions: (a) anode gas recirculation performance and (b) fuel cell stack performance.

6.2. Fuel ejector performance

The most important performance parameters in the fuel ejector obviously are the two mass flow rates, recirculation ratio and STCR. With the new model, these parameters can be analyzed for all the three operational modes.

Keeping the primary flow temperature constant and the anode exhaust condition at the design values as stated in Table 1, the detailed relationships between the two mass flow rates, recirculation ratio, STCR and the primary flow inlet pressure are shown in Fig. 7. It is seen that the mass flow rate of the primary flow increases linearly with the primary flow inlet pressure in accordance with Eq. (6a). However the primary flow inlet pressure has distinct influences on the other performance parameters:

- When the primary flow pressure (P_{PE}) increases up to about 4.45 bar, the secondary flow starts to be entrained into the ejector. The mass flow rate of the secondary flow increases gradually with the primary flow pressure in the subcritical mode, so do the recirculation ratio and STCR.
- The ejector works in the critical mode when the primary flow pressure is greater than 8.47 bar. The mass flow rate of the secondary flow decreases first and then remains quite constant in the high primary flow pressure region.

6.3. Fuel cell performance

First keeping the fuel cell pressure P_{FC} at 3.8 bar and the fuel utilization coefficient U_f at 0.85, the SOFC system performance is studied by varying the other operation conditions as shown in Fig. 8(a) and (b). Then varying P_{FC} and U_f, the off-design behaviors of recirculation ratio and STCR are shown in Fig. 9(a) and (b).

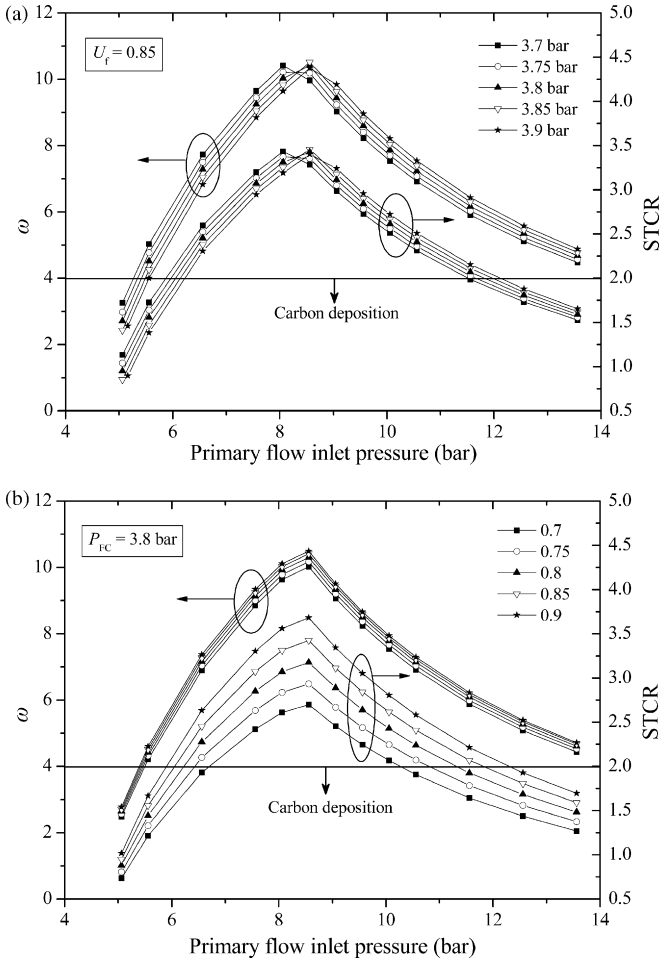

Fig. 9. Performance of a hybrid SOFC at off-design conditions by varying: (a) fuel cell operation pressure and (b) fuel utilization coefficient.

Fig. 8(a) shows the two mass flow rates, recirculation ratio and STCR with the variation of the primary flow inlet pressure. These performance parameters have different behaviors but similar trends with those obtained from Fig. 7. The differences are caused by the temperature and chemical composition of the anode recycle gas which are determined by SOFC operating conditions as shown in Fig. 8(a), while they are always fixed at the design points in Fig. 7.

In Fig. 8(b), the performance parameters of the fuel cell stack: voltage, power and current density are illustrated. It is found that they have the same trends in both the subcritical mode and the critical mode because that these parameters mainly depend on the mass flow rate of the inlet fuel while U_f keeps at the design point. The current density is proportional to the fuel inlet pressure in the subcritical and critical modes. It may be explained that the flow rate of CH_4 into fuel cell stack, $n^{in}_{CH_4}$, increases with the fuel inlet pressure so that $n^{consumed}_{H_2}$ will increase according to Eq. (31), resulting in an increase of the current density. From Fig. 8(b), it is also seen that the FC power increases with the fuel inlet pressure as the $n^{in}_{CH_4}$ is increased while U_f is kept constant. In all the simulated fuel inlet pressure, FC voltage is near 0.53 V.

The recirculation ratio and STCR with the variation of the FC operation pressure is shown in Fig. 9(a). The recirculation ratio and STCR behaviors in the critical mode differ from that in the subcritical mode. The STCR can drop below the limited value for a lower FC pressure in the critical mode, but different in the subcritical mode due to the FC operation pressure has an effect on P_{PE} and P_{PC} as shown in Fig. 6.

Fig. 9(b) shows the results obtained by varying the fuel utilization coefficient at different fuel inlet pressures. The figure indicates that the STCR is strongly influenced by U_f, as U_f has a direct effect on the conversion rate of H_2, which affects the FC performances such as temperature, pressure and chemical composition at the anode recycle gas. Results confirm that for a low U_f, the STCR can easily drop below the limited value and thus suffers from carbon deposition.

7. Conclusions

A theoretical ejector model for performance monitoring and fault detection in the hybrid SOFC system was proposed in this paper. The model was used to analyze the fuel ejector properties such as the primary mass flow rate, the secondary mass flow rate, the recirculation ratio and STCR not only in the critical mode but also subcritical and back flow operational modes. Furthermore, a method for determining P_{PE} and P_{PC}, consequently, the ejector operational mode was introduced.

By utilizing the new model, the performances of an anode gas recirculation SOFC system integrated with a fuel ejector were investigated for the back flow, subcritical and critical operational modes. The main conclusions from the simulation are:

1. Two parameters P_{PE} and P_{PC} which divide the fuel ejector performance into three operational modes should be updated as soon as the fuel cell operating conditions changes.
2. The ejector will not work at the critical mode if the primary flow inlet pressure is less than P_{PC}. In such case, recirculation ratio and STCR need to be carefully monitored.
3. The fuel ejector starts to entrain the secondary flow as the primary flow pressure is about 1.15 times of the ejector exit pressure; reaches the critical mode when the primary flow pressure is approximate 2.2 times of the ejector exit pressure.

References

[1] S.C. Singhal, K. Kendall, High Temperature Solid Oxide Fuel Cells, Elsevier, 2003.
[2] J. Larminie, A. Dicks, Fuel Cell System Explained, John Wiley and Sons Ltd, 2004.
[3] A.L. Dicks, J. Power Sources 61 (1996) 113–124.
[4] T. Takeguchi, Y. Kani, T. Yano, R. Kikuchi, K. Eguchi, K. Tsujimoto, Y. Uchida, A. Ueno, K. Omoshiki, M. Aizawa, J. Power Sources 112 (2002) 588–598.
[5] M.L. Ferrari, A. Traverso, M. Pascenti, A.F. Massardo, Proc. Inst. Mech. Eng. Part A J. Power Energy 221 (2007) 627–635.
[6] M.L. Ferrari, D. Bernardi, A.F. Massardo, J. Fuel Cell Sci. Technol. 3 (2006) 284–291.
[7] I.W. Eames, S. Aphornratana, H. Haider, Int. J. Refrig. 18 (1995) 378–386.
[8] B.J. Huang, J.M. Chang, C.P. Wang, V.A. Petrenko, Int. J. Refrig. 22 (1999) 354–364.
[9] Y.H. Zhu, W.J. Cai, C.Y. Wen, Y.Z. Li, Energ. Convers. Manage 48 (2007) 2533–2541.
[10] F. Marsano, L. Magistri, A.F. Massardo, J. Power Sources 129 (2004) 216–228.
[11] M.L. Ferrari, A. Traverso, L. Magistri, A.F. Massardo, J. Power Sources 149 (2005) 22–32.
[12] Y.H. Zhu, W.J. Cai, C.Y. Wen, Y.Z. Li, J. Power Sources 173 (2007) 437–449.
[13] D.-W. Sun, Energ. Sources 19 (1997) 349–367.
[14] Y. Bartosiewicz, Z. Aidoun, P. Desevaux, Y. Mercadier, Int. J. Heat Fluid Fl. 26 (2005) 56–70.
[15] P. Costamagna, L. Magistri, A.F. Massardo, J. Power Sources 96 (2001) 352–368.
[16] T.G. Benjamin, E.H. Camera, L.G. Marianowski, Handbook of Fuel Cell Performance, Institute of Gas Technology, 1995.